Supplementary Data

L-PBF processing and characterization of a $Ti_{35}Nb_{30}Zr_{29}Mo_3Ta_3$ multiprincipal element alloy for medical implants

Farzin Arjmand,[1*] Adrien Mourgout,[2] Alima Chali,[1] Madjid Djemai,[3] Credson Langueh,[4] Olivier Monasson,[5,6] Elisa Peroni,[5,6] Michel Boissiere,[4] Souad Ammar,[1] Guy Dirras[2]

[1] Université Paris Cité, CNRS UR 7086, ITODYS, 75205 Paris, France
[2] Université Sorbonne Paris Nord, CNRS UPR 3407, LSPM, 93430 Villetaneuse, France
[3] Z3DLAB sas, 95270 Chaumontel, France
[4] CY Cergy Paris Université, ERRMECe, 95000 Cergy Pontoise, France
[5] CY Cergy Paris Université, CNRS, BioCIS, 95000 Cergy Pontoise, France
[6] Université Paris-Saclay, CNRS, BioCIS, 92290 Châtenay-Malabry, France

[*]Corresponding author E-mail address: farzin.arjmand@gmail.com

Elaboration and microstructure/mechanical characterization

The five elemental powders, Ti, Nb, Zr, Mo, and Ta, were spherical powders with over 99% purity, ranging between 10 to 60 µm, in size. The powders were blended following the attended composition and then mixed for 1 h using a 6-axis tubular T_2C. The L-PBF elaboration was achieved using a selective laser melting (SLM) 125HL printer, under Ar atmosphere. The plateau was continuously heated at 200°C and the laser spot was fixed to 80 µm. For the microstructural optimization, over twenty sets of operating parameters were varied. The laser power from 150 to 200 W, the scan speed from 151 to 1200 $mm.s^{-1}$, and the hatching space from 60 to 120 µm. Three sets of processing parameters were selected for further investigation. The samples' laser power, hatching space, and layer thickness were 200 W, 80 and 30 µm, respectively. Scan speeds were adjusted at 555, 185 and 151 $mm.s^{-1}$ for the applied volumetric energy density (VED) of 150, 450 and 550 $J.mm^{-3}$, respectively. Centimeter-sized cubes or parallelepipeds were thus produced, and those retained for the mechanical characterization were then named based on their VED parameter.

In the laser powder bed fusion (L-PBF), the evaporation of the low melting-temperature elements can alter the alloy composition, leading to the formation of pits, particularly in the alloys processed with high VED, as illustrated in Fig.1(c). The inductively coupled plasma mass spectrometry (ICP-MS)

results indeed revealed the existence of some variances between the nominal composition and composition following the applied high VED value.

Table 1S. Nominal and actual L-PBF concentrations of the alloying elements in the VED = 550 J.mm^{-3} alloys, determined by the ICP-MS.

(at. %)	**Ti**	**Nb**	**Zr**	**Ta**	**Mo**
Nominal	39	28	28	2.5	2.5
L-PBF	34.95	30.30	28.66	2.89	3.30
~	35	30	29	3	3

The alloy specimens were first mechanically ground using silicon carbide papers from # 800 to # 2400 grits, then were polished using a 9 µm diamond suspension, followed with a final polishing step with an oxide polishing suspension. A GEMINI 360 (ZEISS) scanning electron microscope (SEM) was then used to determine their grain size and shape. Their orientation was obtained using electron backscatter diffraction (EBSD) on a Supra 40VP (ZEISS) SEM and the data were post-processed with OIM 7.3 software. The dendritic cellular substructure size of the alloys was analyzed with Image J 1.54 g software. Five images for each specimen, representing more than ten thousand cells were considered.

The mechanical micro tensile tests were performed using dog bone specimen geometry, with the dimension of 2 × 1 mm^2 gauge cross-section, thanks to a Deben™ device, coupled with a digital image correlation setup to record the strain. The image correlation was analyzed using the GOM 2019 software. The tensile loading was applied along the X axis (OYZ plane), perpendicular to the SLM building direction (Z axis) at a strain rate of 10^{-3} s^{-1}. The compression tests were conducted with a MTS 20 M machine using 3 × 3 × 5 mm^3 parallelepipedic specimens. The compression loading was applied along the laser beam direction in the Z axis (OXY plane) at a strain rate of 10^{-3} s^{-1}. Each mechanical test was repeated at least three times.

The SEM observations of the elaborated alloys showed the presence of micro-defects in their structures. In the alloys elaborated with low VEDs (Fig. 1S), these defects mainly consist of unmelted Nb/Mo/Ta-rich islands, along with some solidification micro cracks, and a few pits. In comparison with the matrix, these islands have a high density of grain boundaries with low misorientations

(subgrain boundaries). Here it's worth noting that these low angle grain boundaries (LAGBs) are more prevalent in Nb than in Ta and Mo.

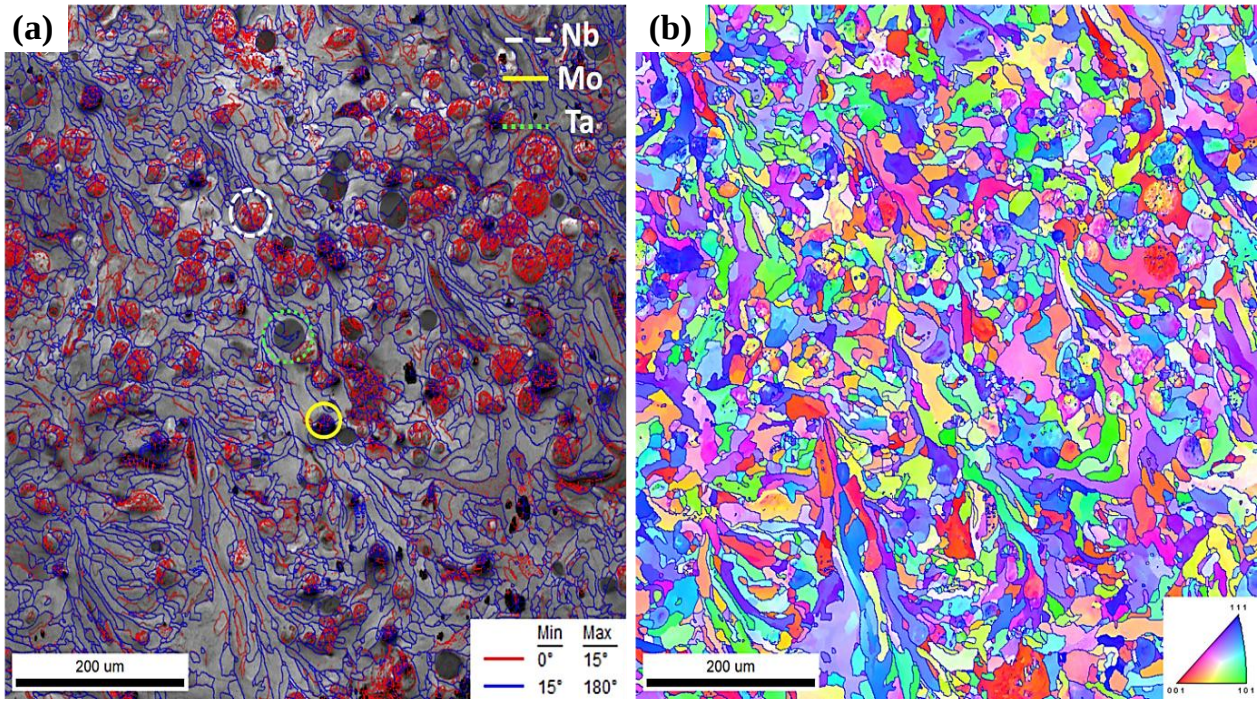

FIG. 1S. EBSD analysis on the OXY plan (a) grain boundary map of the alloy processed at a low VED of 150 J.mm^{-3}, showing a high fraction of LAGBs (red lines/spots) mostly inside the unmelted Nb/Mo/Ta-rich islands and (b) IPF showing the preferred grain orientation in the Nb/Mo/Ta-rich islands.

In contrast, the VED = 550 J.mm^{-3} specimens showed a different pattern with fewer unmelts but a higher proportion of pits/pores.

On the one hand, the presence of porosities and solidification cracks creates points of weakness in the structure of the alloy, which will act as sites favoring the crack initiation and propagation, leading to the final failure of the alloy. Indeed, as shown in Table 2S, the presence of pits in the specimens processed at a higher VED of 550 J.mm^{-3} reduces the tensile ductility of the alloy. (see also [12]). In contrast, the tensile strength of the alloy gets improved due to the improvement in the solid solution strengthening.

On the other hand, the presence of the unmelted Nb/Mo/Ta-rich islands has a significant impact on the solid solution strengthening. Despite their high Young's modulii (105, 329 and 186 GPa, respectively), these islands contribute less to the solid solution strengthening due to their poor solubility in the

matrix. The fact that these alloying elements are not fully diluted in the matrix could be the origin of the observed low value of Young's modulus of about 60 GPa, as shown in Table 2S, compared to 80 GPa for the VED = 550 J.mm^{-3} alloy.

The compressive mechanical properties, particularly the accumulated strain, are usually less sensitive to the processing defects, as shown in Fig. 3. In addition, Table 2S shows that the measured yield strength values are superior to those measured after the tensile tests. Here again, the yield strength values increase with increasing the applied VED due to the enhanced solid solution effect.

Finally, the presence of the unmelted Nb/Mo/Ta islands also significantly effects on the mass density of the alloys. Despite having a lower atomic radius than Zr, these elements are denser: 6.49, 8.57, 10.28 and 16.65 g.cm^{-3} for Zr, Nb, Mo and Ta respectively. Therefore, when they get solubilized in the matrix, they reduce the lattice parameter of the solid solution, leading to an increase in the density. However, one should note that while the increase in the applied VED leads to a rise in the porosity frequency, this factor has a lesser impact on the mass density of the alloys. This is likely because the pits/pores form due to the vaporization of Ti, which is the lighter alloying element here.

Table 2S. Some mechanical parameters of the elaborated alloys versus the applied VED, along with the main detected defects.

	VED = 150 J.mm^{-3}	**VED = 450 J.mm^{-3}**	**VED = 550 J.mm^{-3}**
observed defects	solidification cracks, pits/pores, unmelted Nb/Mo/Ta islands	solidification cracks, pits/pores, unmelted Nb/Mo/Ta islands	solidification cracks, pits/pores, unmelted Nb/Mo/Ta islands
main defect(s)	unmelted Nb/Mo/Ta islands	unmelted Nb/Mo/Ta islands	pits/pores
room temperature tensile properties at a strain rate of $10^{-3}s^{-1}$	Young Modulus = 60 GPa	Young Modulus = 78 GPa	Young Modulus = 80 GPa
	Yield strength = 527 MPa	Yield strength = 950 MPa	Yield strength = 964 MPa
	strength = 674 MPa	strength = 1016 MPa	strength = 1061 MPa
	elongation at break ~15%	elongation at break ~20%	elongation at break ~3%
room temperature compressive properties at a strain rate of $10^{-3}s^{-1}$	Yield strength = 940 MPa	Yield strength = 1215 MPa	Yield strength = 1335 MPa
mass density	6.95 g.cm^{-3}	7.04 g.cm^{-3}	7.07 g.cm^{-3}

The alloy solidification is often accompanied by a microsegregation phenomenon, which is in principle related to the mixing enthalpy ΔHmix. This value is crucial as it determines the tendency of the elements to get mixed or separated during solidification. For example, the ΔHmix between Zr and Ti is 0 $kJ.mol^{-1}$; so Zr and Ti can form an ideal solution. The same applies to Nb and Ta (ΔHmix = 0 $kJ.mol^{-1}$). Here Zr tends to get separated from Nb and Ta due to their high ΔHmix values (4 and 3 $kJ.mol^{-1}$, respectively). The ΔHmix of Mo with Nb/Ta is more negative than that of the ΔHmix of Mo with Ti/Zr. As it can be seen in the SEM-EDS images of Fig. 2S, the dendrites are enriched with Ta, Nb, and Mo (elements with higher melting points), while the inter-dendritic regions contain higher Zr (element with a lower melting point).

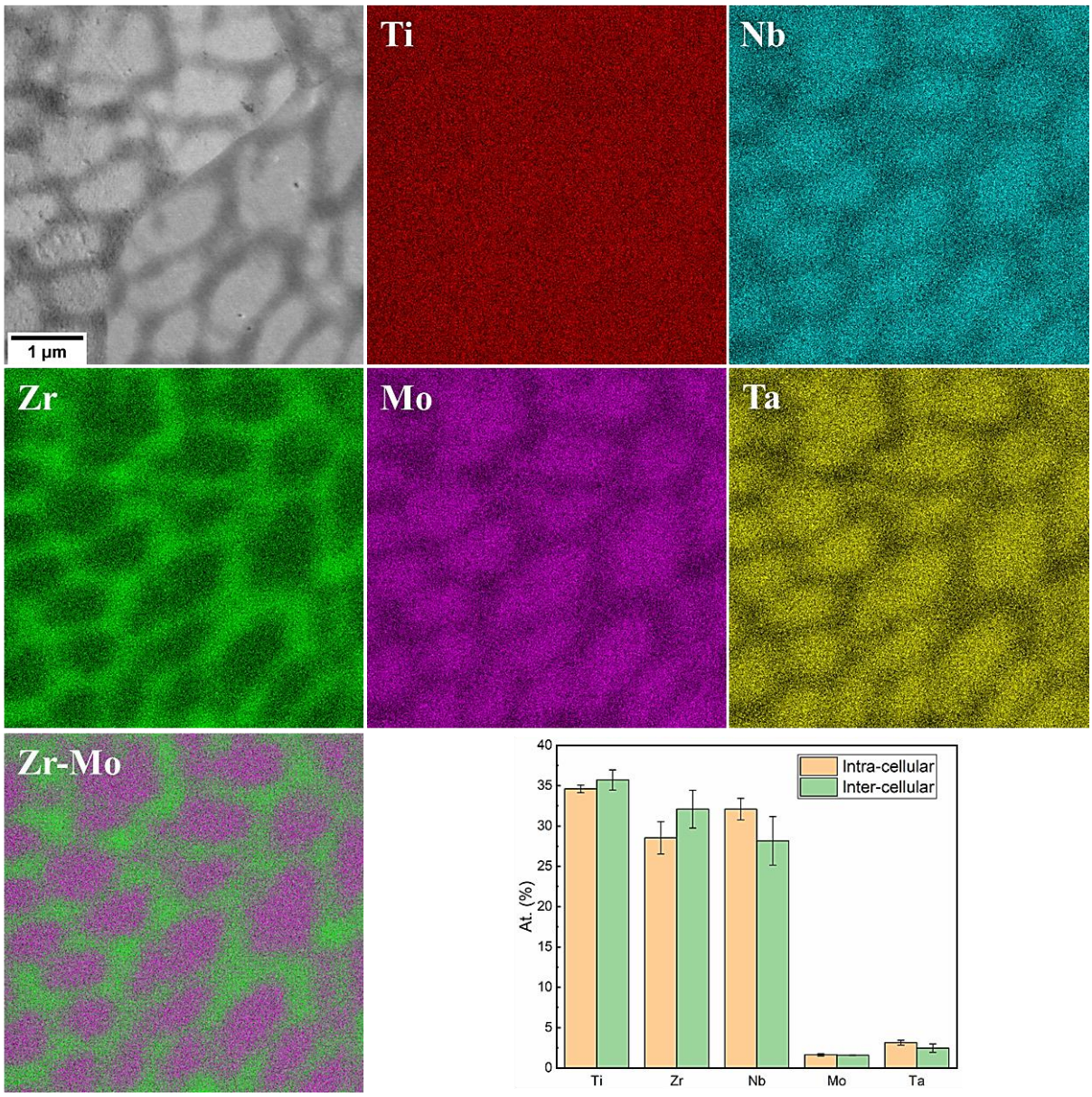

FIG. 2S. SEM-EDS elemental maps of the 550 J.mm^{-3} alloy, showing the distribution of the alloying elements in the dendritic cells.

Electrochemical measurements

For the electrochemical measurements the elaborated alloy specimens were first cut into round coupons of 1 cm in diameter and 2 mm in thickness (s = 0.785 cm^2). Each coupon was then ground with silicon carbide papers with the grit sizes of # 400, # 800, # 1200, # 2000 and # 4000, respectively. The ground coupons then were washed with double distilled water and acetone and cleaned ultrasonically in ethanol for 5 min. The coupons were positioned into a polymeric tube containing

epoxy resin. This way, in the electrochemical cell, only the ground side of each coupon was exposed to the electrolyte.

The electrochemical behavior of the elaborated ground alloy coupons was investigated in a 0.1 M room temperature sodium chloride (NaCl) solution and deoxygenated human body temperature (37°C) glucose rich Gibco Dulbecco's modified eagle medium (DMEM) supplemented or not with 20% of fetal bovine serum (FBS).

The potentiodynamic polarization curves and electrochemical impedance spectroscopy (EIS) plots were recorded using a BioLogic SP-150 (Science Instruments) potentiostat, in a three electrode setup with a Ag/AgCl/KCl (sat.) reference electrode, a graphite rod as counter electrode and the alloy coupons as working electrode. After immersing each working electrode into the different electrolytes, its open circuit potential (OCP) was monitored, until reaching a stable value. The working electrode was then potentiodynamically polarized by scanning its potential from a cathodic potential, a few mV more negative than its OCP to +1.6 V vs. Ag/AgCl/KCl (sat.) with the scan rate of 1 $mV.s^{-1}$. The Nyquist plots were recorded in the frequency range from 100 kHz to 10 mHz with an amplitude of 1 mV. Here, considering the different cell temperatures, all the measured potentials were converted to *E* vs. Standard Hydrogen Electrode (SHE).

In Fig. 3S(a-d), the Bode total impedance ($|Z|$) versus frequency plots of the 150 and 550 $J.mm^{-3}$ alloys, the potentiodynamic polarization curves of the 150 $J.mm^{-3}$ alloy coupons, as well as the Nyquist plots of the 150 $J.mm^{-3}$ alloy (all in the OXY plane), recorded after 24 h exposure to 0.1 M NaCl (25°C), deoxygenated DMEM (37°C) and deoxygenated DMEM + FBS (80:20 (v/v)) (37°C) media can be observed. Comparing the electrochemical data presented in these figures with the corrosion parameters of the 550 $J.mm^{-3}$ alloy depicted in Fig. 4(a, b), it is obvious that in all the exposed electrolytes the 150 $J.mm^{-3}$ alloy has a more negative OCP (E_{corr}), a larger oxidation/dissolution current density and a lower impedance (real, imaginary and total) values. This shows the lower resistivity of the 150 $J.mm^{-3}$ alloy to corrosion, compared to the alloy elaborated with the VED of 550 $J.mm^{-3}$.

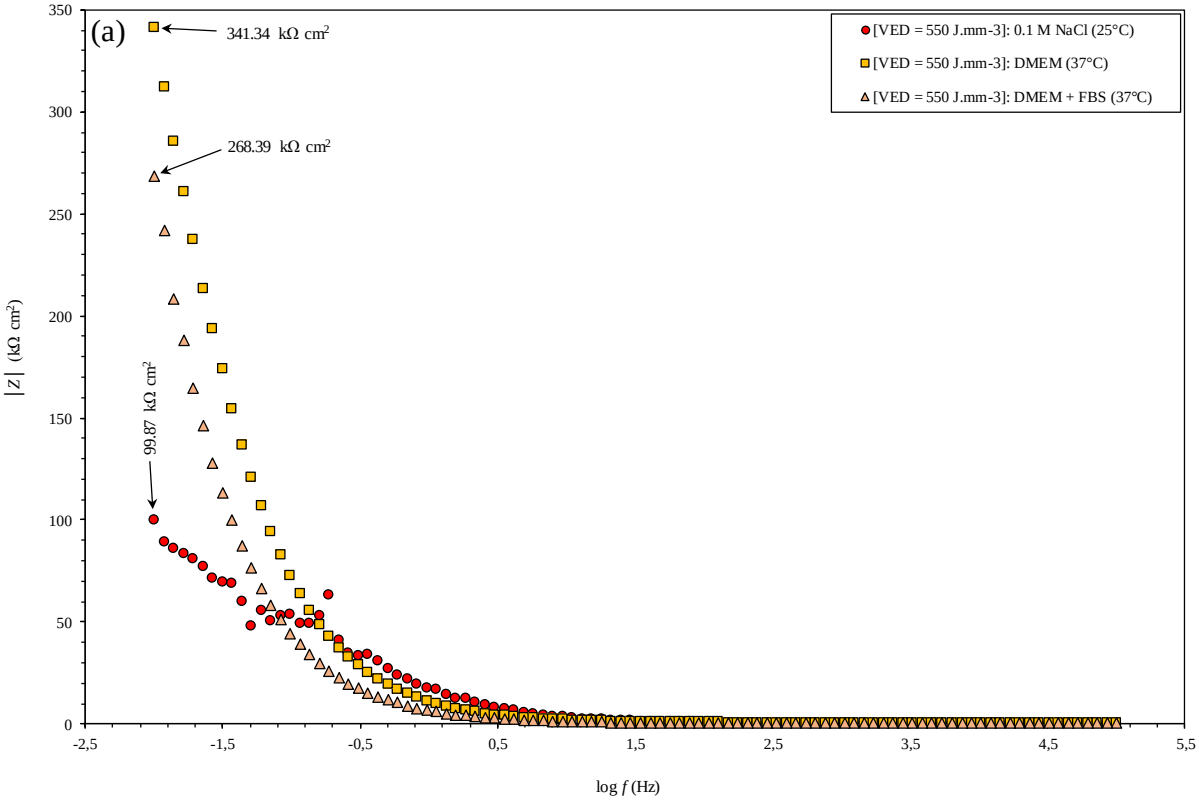
(a)
341.34 kΩ cm²
268.39 kΩ cm²
99.87 kΩ cm²
[VED = 550 J.mm-3]: 0.1 M NaCl (25°C)
[VED = 550 J.mm-3]: DMEM (37°C)
[VED = 550 J.mm-3]: DMEM + FBS (37°C)
|Z| (kΩ cm²)
log f (Hz)

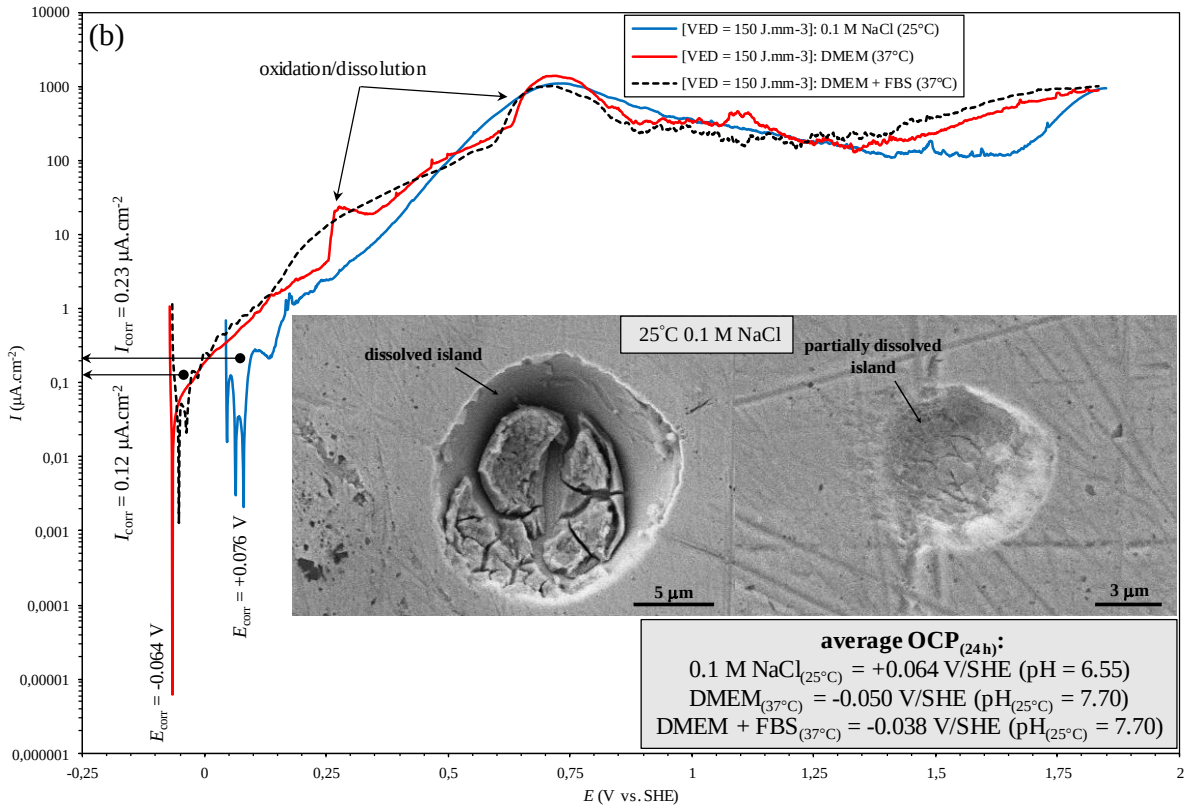
(b)
[VED = 150 J.mm-3]: 0.1 M NaCl (25°C)
[VED = 150 J.mm-3]: DMEM (37°C)
[VED = 150 J.mm-3]: DMEM + FBS (37°C)
oxidation/dissolution
I_corr = 0.23 µA.cm-2
I_corr = 0.12 µA.cm-2
E_corr = +0.076 V
E_corr = -0.064 V
25°C 0.1 M NaCl
dissolved island
partially dissolved island
5 µm
3 µm
average OCP(24h):
0.1 M NaCl(25°C) = +0.064 V/SHE (pH = 6.55)
DMEM(37°C) = -0.050 V/SHE (pH(25°C) = 7.70)
DMEM + FBS(37°C) = -0.038 V/SHE (pH(25°C) = 7.70)
I (µA.cm-2)
E (V vs. SHE)

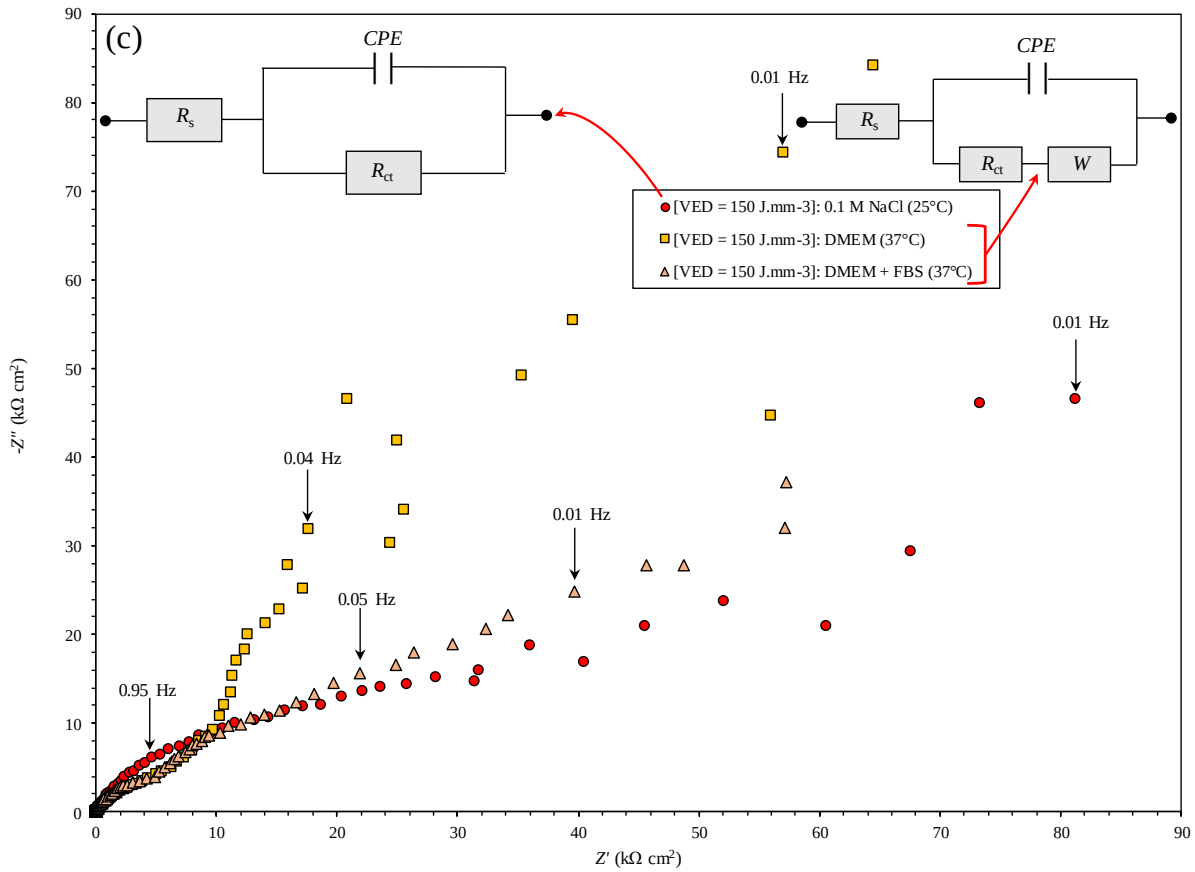
(c)
CPE
R_s
R_{ct}
0.01 Hz
CPE
R_s
R_{ct}
W
[VED = 150 J.mm-3]: 0.1 M NaCl (25°C)
[VED = 150 J.mm-3]: DMEM (37°C)
[VED = 150 J.mm-3]: DMEM + FBS (37°C)
0.01 Hz
0.04 Hz
0.01 Hz
0.05 Hz
0.95 Hz
-Z'' (kΩ cm²)
Z' (kΩ cm²)

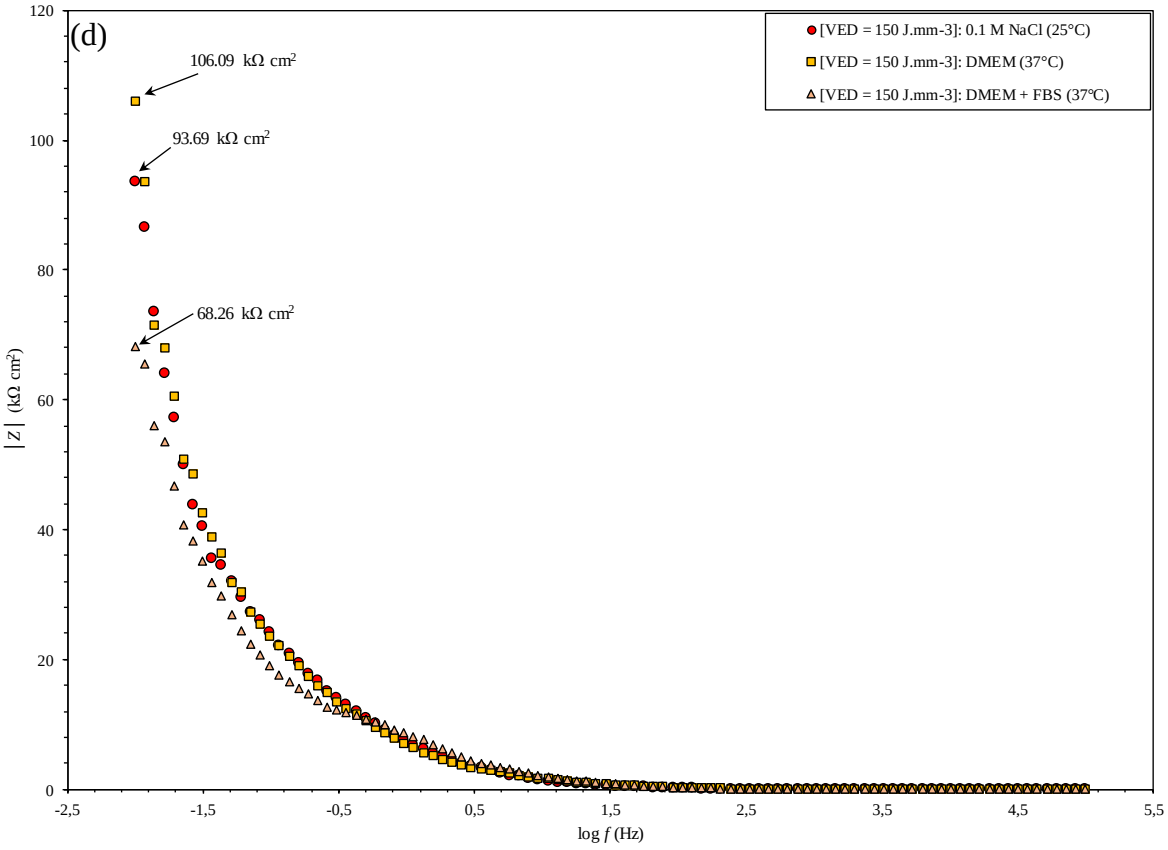
(d)
[VED = 150 J.mm-3]: 0.1 M NaCl (25°C)
[VED = 150 J.mm-3]: DMEM (37°C)
[VED = 150 J.mm-3]: DMEM + FBS (37°C)
106.09 kΩ cm²
93.69 kΩ cm²
68.26 kΩ cm²
|Z| (kΩ cm²)
log f (Hz)

FIG. 3S. (a) Bode $|Z|$ versus frequency plots of the 550 J.mm^{-3} and (b-d) potentiodynamic polarization curves, Nyquist and Bode $|Z|$ versus frequency plots of the 150 J.mm^{-3} alloy coupons (in the OXY plane), recorded after 24 h exposure to 0.1 M NaCl (25°C), deoxygenated DMEM (37°C) and deoxygenated DMEM + FBS (80:20 (v/v)) (37°C) media, showing the lower resistivity of the 150 J.mm^{-3} alloy to corrosion compared to the 550 J.mm^{-3} alloy in all the exposed media. The inset: SEM images in Fig (b) show the pits, nucleated on the surface of the 150 J.mm^{-3} coupon during its polarization in the NaCl solution.

Fig. 4S presents some more SEM images of the alloy coupons after being electrochemically polarized in the NaCl, DMEM and DMEM + FBS electrolytes. In general, three different areas are distinguishable in all the images. These are (i) intact Nb/Mo/Ta-rich islands, (ii) partially dissolved islands and (iii) completely dissolved islands. The latter forms round and relatively large pits on the surface of the coupons. Similar pits were found on the 550 J.mm^{-3} coupon, after being polarized in the 37°C deoxygenated DMEM + FBS electrolyte.

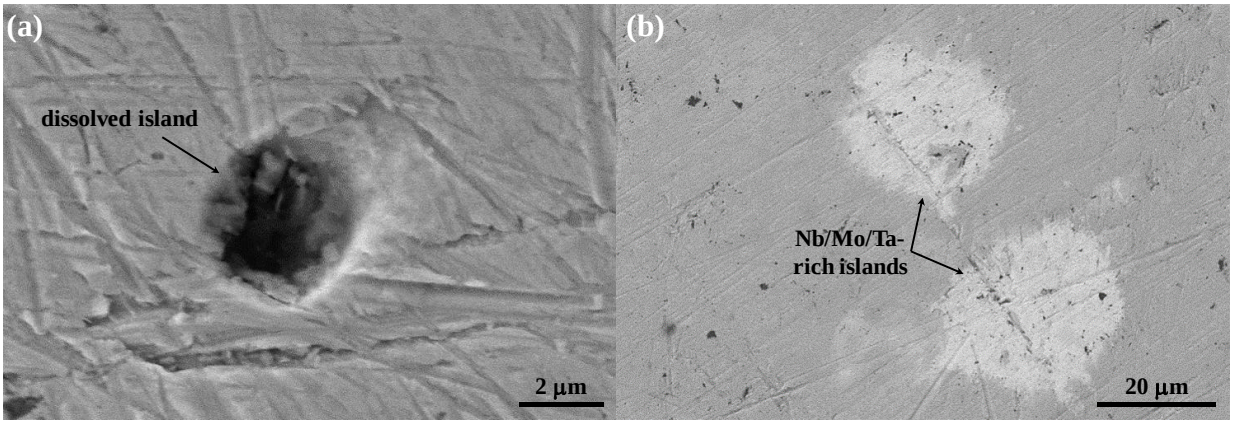

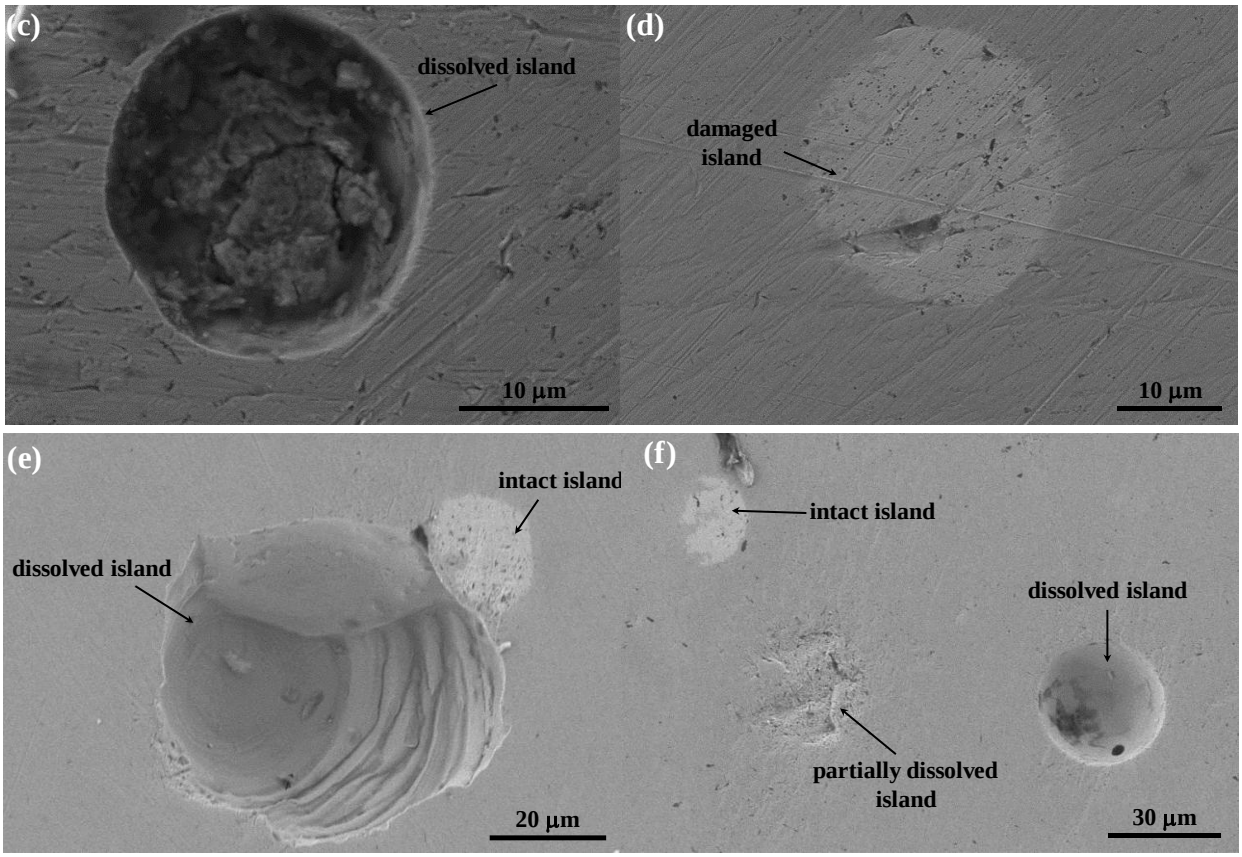

FIG. 4S. SEM images of the intact/partially dissolved Nb/Mo/Ta islands and pits formed on the (a, b) 150 J.mm^{-3} in DMEM, (c, d) 150 J.mm^{-3} in DMEM + FBS and (e, f) 550 J.mm^{-3} in 0.1 M NaCl.

Cytotoxicity tests in conditioned medium

Conditioned mediums were prepared by immersing freshly prepared circular coupons for 24 h in 10 mL of a 1:1 mixture of DMEM and Ham's F_{12} media (DMEM:F_{12}). This formulation combines DMEM's high concentrations of glucose, amino acids, and vitamins with the wide variety of components found in Ham's F_{12} media DMEME. Pre-osteoblastic mousse cells MC_3T_3-E_1, obtained from the American Type Culture Collection (ATCC, Manassas, VA), were cultured at 37°C in an atmosphere containing 5% CO_2 in a Thermo Forma incubator (Thermo Fisher, Waltham, MA). The control cells were grown in the DMEM:F_{12} medium (ATCC) supplemented with a 10% fetal bovine serum and a 50 µg.mL^{-1} penicillin/streptomycin (ATCC), which was identical to the medium used for the cytotoxicity tests, except for the exposure to the alloy discs. In both instances, MC_3T_3-E_1 cells were seeded at a density of 20,000 cells per well in a 24-well plate.

To determine the cell proliferation, the previous samples were fixed for 15 min with a 4% paraformaldehyde (Sigma-Aldrich) solution in a phosphonate saline buffer (PBS). Cells were then

labeled for 30 min with a solution containing a 10 µg.mL^{-1} of 4′ ,6-diamidino-2-phenylindole dihydrochloride (DAPI, Sigma-Aldrich) to stain their nucleus. The cellularized supports were examined using a Leica fluorescence microscope (10X objective). For each sample, 3 independent fields were analyzed. The experiments were repeated thrice. The given data are representative of the three different experiments performed in duplicate. The image post-processing was performed using the Fiji 2.9.0 software.

To address the MC_3T_3 morphology evolution, the cells were seeded in a 24-well plate and cultured for 3, 24, and 48 h in two different conditioned and control (free of alloy exposure) media. Initially, the cells were fixed using a 4% paraformaldehyde solution for 10 min and subsequently rinsed with PBS. The cells were then permeabilized with a 0.2% (v/v) PBS-Triton X-100 solution for 5 min, followed by another rinse with PBS. Each substrate was incubated for 30 min in a blocking buffer of PBS–BSA 5% (w/v). The substrates were then incubated for 1 h at room temperature with DAPI (10 µg/mL) and AlexaFluor 568-phalloidin conjugate (diluted 1/400) (Thermo Fisher Scientific, Illkirch, France) to stain the cell nucleus and actin cytoskeleton respectively. After thorough rinsing, the substrates were mounted on each sample using a Prolong Gold® antifade mountant. Observations and image acquisition were conducted using a Confocal Laser Scanning Microscope (CLSM), LSM 900 (Zeiss), equipped with objectives of 20X or 63X magnification. For each sample, three independent fields were analyzed. The image post-processing was performed using Fiji 2.9.0 software.

Cell culture

Cytotoxicity tests in conditioned medium

The alloy composition under study was $Ti_{35}Nb_{30}Zr_{29}Mo_3Ta_3$. The conditioned media were prepared by immersing the alloy coupons (1 cm in diameter, 2 mm thick) in a 10 mL of DMEM:F_{12} medium for 24 h. The MC_3T_3-E_1 cells, obtained from the American Type Culture Collection (ATCC, Manassas, VA), were cultured at 37°C in an atmosphere containing 5% CO_2 in a Thermo Forma incubator (Thermo Fisher, Waltham, MA). The Control cells were grown in the DMEM:F_{12} medium (ATCC) supplemented with a 10% fetal bovine serum (FBS) and a 50 µg/mL penicillin/streptomycin (ATCC),

which was identical to the medium used for the cytotoxicity tests, except for the exposure to the alloy coupons. In both instances, the MC_3T_3-E_1 cells were seeded at a density of 20,000 cells per well in a 24-well plate.

Cell proliferation

To determine the cell proliferation, the previous samples were fixed for 15 min with a 4% paraformaldehyde (Sigma-Aldrich) solution in PBS. The cells were then labeled for 30 min with a solution containing 10 µg/mL of 4′ ,6-diamidino-2-phenylindole dihydrochloride (DAPI, Sigma-Aldrich). The cellularized supports were examined using a Leica fluorescence microscope (10X objective). For each sample, 3 independent fields were analyzed. The obtained data were representative of three different experiments performed in duplicate. The image post-processing was performed using Fiji® software (2.9.0 version).

Cell morphology analysis

The MC_3T_3 cells were seeded in a 24-well plate and cultured for 3, 24, and 48 h in the conditioned and control (free of alloy exposure) media. Initially, the cells were fixed using a 4% paraformaldehyde solution for 10 min and subsequently rinsed with PBS. The cells were then permeabilized with a 0.2% (v/v) PBS-Triton X-100 solution for 5 min, followed by another rinse with PBS. Each substrate was incubated for 30 min in a blocking buffer of PBS–BSA 5% (w/v). The substrates were then incubated for 1 h at room temperature with a DAPI (10 µg/mL) and a AlexaFluor 568-phalloidin conjugate (diluted 1/400) (Thermo Fisher Scientific, Illkirch, France). After thorough rinsing, the substrates were mounted on each sample using a Prolong Gold® antifade mountant. The observations and image acquisition were conducted using a Confocal Laser Scanning Microscope (CLSM), LSM 900 (Zeiss), equipped with objectives of 20X or 63X magnification. For each sample, three independent fields were analyzed. The image post-processing was performed using Fiji® imaging software.